Identification of Zonal Flows in a Toroidal Plasma

A. Fujisawa,[1] K. Itoh,[1] H. Iguchi,[1] K. Matsuoka,[1] S. Okamura,[1] A. Shimizu,[1] T. Minami,[1] Y. Yoshimura,[1] K. Nagaoka,[1]
C. Takahashi,[1] M. Kojima,[1] H. Nakano,[1] S. Ohsima,[1] S. Nishimura,[1] M. Isobe,[1] C. Suzuki,[1] T Akiyama,[1] K. Ida,[1] K. Toi,[1]
S.-I. Itoh,[2] and P. H. Diamond[3]

[1]*National Institute for Fusion Science, Oroshi-cho, Toki-shi, 509-52 Japan*
[2]*RIAM, Kyushu University, Kasuga, 816 Japan*
[3]*University of California, San Diego, La Jolla, California 92093-0319, USA*

This Letter presents experimental confirmation of the presence of zonal flows in magnetically confined toroidal plasma using an advanced diagnostic system—dual heavy ion beam probes. The simultaneous observation of an electric field at two distant toroidal locations (~ 1.5 m apart) in the high temperature (~ 1 keV) plasma provides a fluctuation spectrum of electric field (or flow), a spatiotemporal structure of the zonal flows (characteristic radial length of ~ 1.5 cm and lifetime of ~ 1.5 ms), their long-range correlation with toroidal symmetry ($n = 0$), and the difference in the zonal flow amplitude with and without a transport barrier. These constitute essential elements of turbulence-zonal flow systems, and illustrate one of the fundamental processes of structure formation in nature.

Zonal flows—azimuthally symmetric bandlike shear flows—are ubiquitous phenomena in the Universe [1–3]; examples include Jovian belts and zones, the terrestrial atmospheric jet stream, the super-rotation of the Venusian atmosphere, and the rotation profile of the solar tachocline. Zonal flows have been expected to be present in magnetically confined toroidal plasmas [4] since the characteristics of drift wave turbulence in the plasmas are analogous to Rossby wave turbulence to cause the phenomena in the rotating planets. Recently, their crucial role in determining the turbulent level and resultant transport has been widely recognized, and the identification of the zonal flows becomes an urgent issue in the fusion research to enhance the prospect of plasma burning in the International Thermonuclear Experimental Reactor [5–7].

In toroidal plasmas, the zonal flows emerge in electric field fluctuation symmetric ($m = n = 0$) on magnetic flux surface with finite radial wave numbers (see for review, e.g., [8,9]). Two major branches of zonal flows are expected in magnetic confined toroidal plasmas, i.e., a residual flow of nearly zero frequency, and an oscillatory flow termed geodesic acoustic modes (GAMs) [10,11]. These zonal flows are driven *exclusively* by nonlinear interactions (or inverse cascade) through energy transfer from the microscopic drift waves. Inversely, the zonal flows regulate the drift wave turbulence and resultant transports. The time-varying $E \times B$ shearing of zonal flows, similar to the mean flows [12], has a significant effect on plasma turbulence and transport.

Direct nonlinear simulations have, in fact, confirmed the appearance of and generation processes for zonal flows [13–20], and their essential role in turbulence and transport of toroidal plasmas. In experiments, however, only indirect signs have been obtained for zonal flows and their role in confinement. Coherent oscillations presumed to be GAMs were detected in measurements with a heavy ion beam probe (HIBP) [21,22], with traditional probes [23,24], and with beam emission spectroscopy using a modified time-delayed-estimation analysis technique [25]. Bicoherence analysis showed an increase in nonlinear interaction between zonal flows and turbulence during *L*-to-*H* transition, suggesting a role of turbulent Reynolds stress in zonal flow generation [26,27]. In this Letter, we describe a direct identification of zonal flows in a toroidal plasma with their fundamental characteristics.

The stage of our experiments is a helical device (stellarator), named compact helical system (CHS), with the major and averaged minor radii being $R = 1$ m and $a = 0.2$ m, respectively. The target plasma is produced with electron cyclotron resonance heating of ~ 200 kW, for avoiding magnetohydrodynamics behavior that may interfere with the zonal flow detection. The plasma parameters are magnetic field strength $B = 0.88$ T, density $n_e \simeq 5 \times 10^{12}$ cm^{-3}, electron temperature $T_e \simeq 1$ keV, ion temperature $T_i \simeq 0.1$ keV, ion Larmor radius $\rho_i \sim 0.1$ cm, time scale of microinstabilities $\omega^* \sim 50$ kHz with $k_\perp \rho_i = 0.3$, and energy confinement time $\tau_E \sim 2.5$ ms (or the characteristic frequency $\tau_E^{-1}/2\pi \sim 0.1$ kHz).

The potential and density fluctuations of the CHS plasma are measured with two HIBPs [28]. In our case, accelerated cesium beams of a singly ionized state are injected into the plasma. Doubly ionized beams produced through electron impact collisions in the plasma are detected with an energy analyzer. The energy difference between the injected and detected beams corresponds to the plasma potential at the ionization point. The fluctuation in detected beam intensity brings information of local density fluctuation at the ionization point, although the signal is contaminated with density fluctuation along beam orbit to some extent according to the operational condition.

As is shown in Fig. 1(a), the HIBPs are located apart from each other by approximately 90° in a toroidal direction. Each of them is capable of measuring three adjacent positions in the plasma. Two calculations of *electric field* (or potential difference), $\Delta\phi_{in} = -\phi_{in} + \phi_{ctr}$ and $\Delta\phi_{out} = -\phi_{ctr} + \phi_{out}$, can be made from potentials at three channels denoted as ϕ_{in}, ϕ_{ctr}, and ϕ_{out}. The radial electric field can be estimated from the quotient of the potential difference by the sample volume distance; $E = \Delta\phi/\Delta r_{eff}$ where Δr_{eff} means the distance between magnetic flux surfaces on which the centers of gravity of the sample volumes lie. The necessary cesium beam energy is ~70 keV for the experimental condition.

Figure 1(b) shows overall characteristics of power spectra in potential difference. The measured radial position is $r_{obs} = 12 \pm 0.5$ cm or two-thirds of the plasma minor radius. A spectrum is evaluated as an ensemble average for a stationary period of ~80 ms in a discharge duration of ~100 ms. The elements are calculated using the fast Fourier transform (FFT) technique for sequential windows taken from the stationary period.

The solid red line in Fig. 1(b) shows a shot-averaged spectrum of potential difference from an HIBP, $\Delta\phi(r_2)$, with a frequency resolution of ~0.24 kHz (i.e., a window contains 2^{11} data points). The sampling rate of 2 μs gives the Nyquist frequency of 250 kHz. The spectrum is significantly above the noise level in a wide range of frequency. Another shot-averaged spectrum (the dashed red line) is calculated with a high frequency resolution of ~0.06 kHz to see the tendency in the lower frequency of $f \lesssim 0.4$ kHz by taking longer FFT windows of 2^{13} data points (but poorer statistics). It is found that the power spectrum should reach a maximum at $f = 0.3$–0.7 kHz.

As is represented by the blue line, the fluctuation in this low frequency range shows a high coherence (~0.6) between two toroidal locations. The coherence is analyzed with the low frequency resolution for better statistics; the coherence can become closer to one in an appropriate period of a single shot. Figure 1(c) shows an example of the phase difference (divided by π) when the observation points are located on a flux surface. The phase difference is regarded as zero within the present error bars, and clearly shows the toroidally symmetric structure of $n = 0$; the toroidal structure of $n = \pm1$ should give the phase shift of $\pi/2$ in our diagnostics geometry. Consequently, the activity of potential difference in this frequency range, demonstrating a long distance correlation, is the zonal flow of concern.

A sharp peak is found at $f = 16.5$ kHz with a width of ~1 kHz. Figure 1(d) shows an expanded view around the peak. The theoretically expected GAM frequency is $c_s/2\pi R \sim 17$ kHz in this experimental condition, with c_s being the ion sound velocity. Poorer signal-to-noise ratio of the other HIBP signal cannot allow further inspection of the long-range correlation of this mode at present. On the other hand, the spectrum around $f \sim 50$ kHz shows turbulent characteristics of a broad peak with the half width of 18.5 ± 1.4 kHz. The power of residual zonal flow decays as $P \propto f^{-0.6}$ in the intermediate range of frequency toward the regime of turbulence waves which may generate the zonal flows.

Dynamics of electric field of the residual zonal flow can be visualized with a numerical filter to extract the corresponding frequency activity. The numerical filter used here is described as $\tilde{x}(t) = \int_{t-\infty}^{t+\infty} w(t - t')x(t')dt'$, where $w(t - t', \tau_f) = (1/\sqrt{2\pi\tau_f^2})\exp[-(t - t')^2/2\tau_f^2]$. The time constant for high frequency cutoff is selected as $\tau_f = 0.3$ ms here. The extremely low frequency is also removed to avoid the effects of plasma movement or changes in plasma parameters using the filter with $\tau_f = 1$ ms. The resultant filter property has a peak around 0.5 kHz with the width of ~1 kHz in the frequency domain.

Figure 2 shows two examples of processed potential difference $\Delta\phi$. One is the time evolution of the potential difference at the points localized on the same magnetic flux surface [Fig. 2(a)]. The others are on slightly
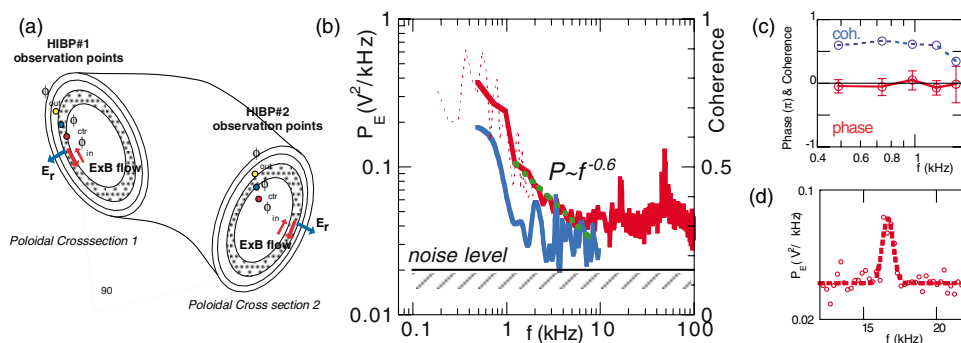

FIG. 1 (color). (a) Geometry and observation points of dual heavy ion beam probes in CHS. (b) Power spectra of potential difference (red lines), and coherence between potential differences (blue line) at the two toroidal locations. The electric field fluctuation ranging from 0.3 to 1 kHz shows long-range correlation, and reflects the activity of the zonal flow of nearly zero frequency. The hatched region shows the noise level for power. (c) An example of phase (divided by π) and coherence between potential differences at two toroidal locations on a magnetic flux surface. (d) An expanded view of a sharp peak at $f = 16.5$ kHz.
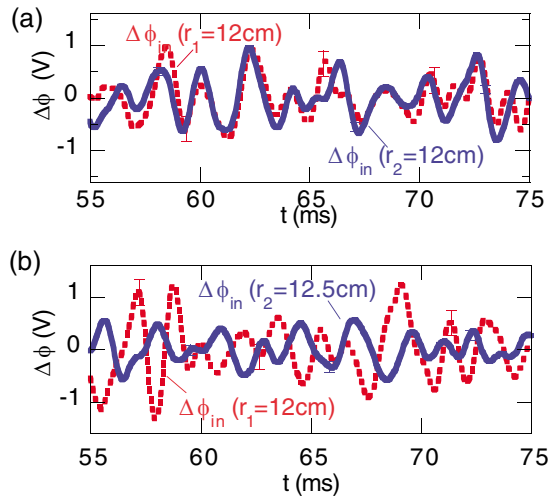
FIG. 2 (color online). Time evolution of zonal flow. (a) Waveforms of electric field (or potential difference) on the same magnetic flux surface in different toroidal positions. (b) Waveforms of electric field (or potential difference) on slightly different magnetic flux surface in different toroidal positions.

different locations displaced by 5 mm [Fig. 2(b)] in a radial direction. The waveforms in both cases alter temporally in a synchronized way but differently in phase. Obviously, the phase differences of the first and second cases are in and out of phases, respectively. The autocorrelation analysis of the waveform allows one to estimate the lifetime of the residual zonal flow. The average of a dozen shots yields $\tau_{auto} = 1.4 \pm 0.2$ ms.

The waveforms indicate that the fluctuation amplitude of ~ 1 V. This follows that the absolute value of the zonal electric field (or the zonal flow velocity) is 0.05–0.1 kV/m (or 0.06–0.11 km/s) from the sample volume distance obtained in the trajectory calculation, $\Delta r_{eff} \sim 1.5 \pm 0.5$ cm; cf. the mean radial electric field (or mean flow) at the position of $r = 12$ cm is ~ 1 kV/m (or ~ 1.1 km/s). The error bar comes from the change in the center of gravity of sample volumes due to the beam focusing property. The electric field can be 2 times larger by taking into account the effect of the sample volume average.

The waveforms without any phase shift in Fig. 2(a) clearly demonstrate the toroidal symmetry ($n = 0$) of electric field fluctuation. The fact is also circumstantial evidence to support the poloidal symmetry ($m = 0$) as follows. By tracing the magnetic field line, an observation point of an HIBP can be projected onto the poloidal cross section in which another observation point of the other is located. The electric field fluctuations at these two points with a finite poloidal angle should be in phase if one assumes that electric field fluctuations are coherent on a magnetic field line. This consideration verifies the poloidal symmetry in the range of the poloidal angle approximately from 30° ($r = 4$ cm) to 50° ($r = 12$ cm), since the existence of toroidal symmetry in the zonal flow activity

has been already confirmed for other magnetic flux surfaces ($r = 4$–12 cm) in our experiments.

The measurements of phase difference hint a possibility to infer a radial structure of the residual zonal flow by altering the observed position of potential difference, r_2, while fixing the other at r_1. The phase between electric fields at two locations can be deduced from traditional correlation coefficient and the FFT analysis of coherence and phase. The correlation between the potential differences, $C(r_1, r_2) = \langle \Delta\phi(r_1) \cdot \Delta\phi(r_2) \rangle / \sqrt{\langle \Delta\phi(r_1)^2 \rangle \cdot \langle \Delta\phi(r_2)^2 \rangle}$ is evaluated where $\langle \psi \rangle = (1/2T) \times \int_{t-T}^{t+T} \psi dt$. Figure 3 shows the correlation coefficient (closed circles) as a function of the observation position r_2. The plotted values are the ensemble averages of the correlation coefficients for time windows in stationary states.

The open circles in Fig. 3 show the other indicators to reflect the structure, that is, $\langle \gamma \cos\theta \rangle_f$ (an average of the frequencies in the range of $0.5 < f < 1$ kHz), where γ and θ are the coherence and phase difference in the FFT analysis. Both analyses demonstrate a sinusoidally changing structure. In the latter case, a Fourier transformation on $\gamma \cos\theta$ curves of individual frequencies allows us to give an averaged wavelength of $\lambda = 1.6 \pm 0.2$ cm. This corresponds to approximately 15 times ion Lamour radius and shorter than one-tenth of plasma minor radius. The wave number allows one to give a rough estimation of the shearing rate of the zonal flow being as $\omega_{E \times B} \sim k_r \tilde{E}/B = 0.3 \times 10^5$ s^{-1}, while the turbulence decorrelation rate could be $\gamma_{turb} \sim 1.2 \times 10^5$ s^{-1} from the width of the broadband spectrum around ~ 50 kHz.

Besides, a prospective result has been obtained to indicate the relation between zonal flow and confinement. A clear difference is recognized between the amplitude of the zonal flow among cases with and without a transport
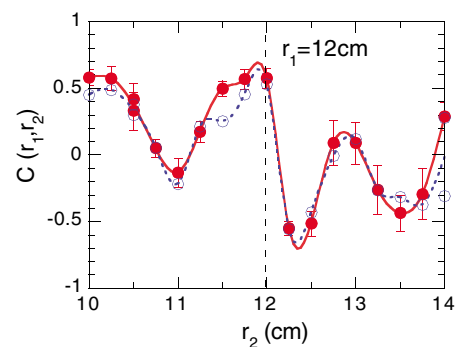

FIG. 3 (color online). Radial structure of zonal flow. The structure is estimated from correlation between potential differences at different toroidal locations. In this experiment, the observation radius of the second HIBP is varied around $r_2 = 12$ cm with the observation point of the first HIBP being fixed at $r_1 = 12$ cm. The closed circles represent the traditional correlation coefficient as a function of the observation radius of the second HIBP, while the open circles do coherent structure from FFT analysis.

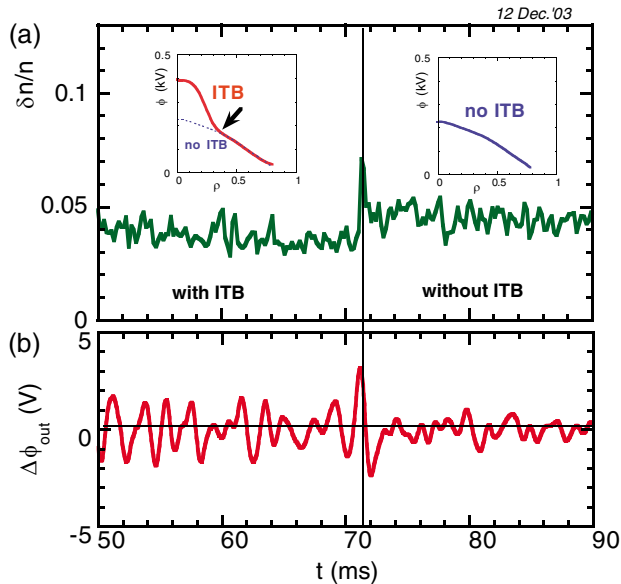165002-3   165002-3

FIG. 4 (color online). Zonal flow with and without a transport barrier. (a) A change of density fluctuation amplitude, and (b) a change in zonal flow amplitude before and after a transition. The potential profiles before and after the transition are shown as insets. The solid vertical line indicates the transition time. The arrow in the left inset indicates the observation point.

barrier. Figure 4 shows an example of a change in zonal flow amplitude before and after a back transition; here the internal transport barrier (ITB) [29] decays with the back transition, and potential profiles before and after the transition are shown as insets. In the transition, the mean value of radial electric field is changed from ~8 to ~1 kV/m. After the back transition happens, the zonal flow amplitude decreases, simultaneously with an increase in the density fluctuation amplitude (on the barrier foot point, $\rho = 0.3 \pm 0.05$) in the frequency range of more than $f \sim 2$ kHz. This observation—the ITB characterized by stronger zonal flow—suggests an interplay between zonal flow and turbulence fluctuation.

Finally, we have described the dual HIBP measurements to show the presence of the zonal flows and their fundamental characteristics in a toroidal plasma. Our discovery of the zonal flows gives a basic insight into plasma and rotating fluid transport. Plasmas in laboratory provide opportunities to study nonlinear processes, between turbulence and zonal flow, playing an essential role in structural formation in the Universe.

[1] F. H. Busse, Chaos **4**, 123 (1994).
[2] P. S. Marcus, T. Kunda, and C. Lee, Phys. Plasmas **7**, 1630 (2000).
[3] E. A. Spiegel, and J.-P. Zahn, Astron. Astrophys. **265**, 106 (1992).
[4] A. Hasegawa, C. G. Maclennen, and Y. Kodama, Phys. Fluids **22**, 2122 (1979).
[5] J. Glanz, Science **274**, 1600 (1996).
[6] Z. Lin, T. S. Hahm, W. W. Lee, W. M. Tang, and R. B. White, Science **281**, 1835 (1998).
[7] M. N. Rosenbluth and F. L. Hinton, Phys. Rev. Lett. **80**, 724 (1998).
[8] P. H. Diamond, K. Itoh, S.-I. Itoh, and T. S. Hahm (to be published).
[9] A. Yoshizawa, S.-I. Itoh, and K. Itoh, *Plasma and Fluid Turbulence* (Institute of Physics Publishing, Bristol and Philadelphia, 2003).
[10] N. Winsor, J. L. Johnson, and J. M. Dawson, Phys. Fluids **11**, 2448 (1968).
[11] K. Hallatschek and D. Biskamp, Phys. Rev. Lett. **86**, 1223 (2001).
[12] H. Biglari, P. H. Diamond, and P. W. Terry, Phys. Fluids B **2**, 1 (1990); K. Itoh, S.-I. Itoh, A. Fukuyama, H. Sanuki, and M. Yagi, Plasma Phys. Controlled Fusion **36**, 123 (1994).
[13] P. H. Diamond *et al.*, in *Proceedings of the 17th IAEA Fusion Energy Conference, Yokohama, 1998* (International Atomic Energy Agency, Vienna, Austria, 1999), Vol. 4, pp. 1421–1428.
[14] A. Hasegawa and M. Wakatani, Phys. Rev. Lett. **59**, 1581 (1987).
[15] G. Hammet *et al.*, Plasma Phys. Controlled Fusion **35**, 973 (1993).
[16] R. E. Waltz, G. D. Kerbel, and J. Milovich, Phys. Plasmas **1**, 2229 (1994).
[17] A. M. Dimits *et al.*, Phys. Plasmas **7**, 969 (2000).
[18] K. Hallatschek, Phys. Rev. Lett. **84**, 5145 (2000).
[19] B. D. Scott, Phys. Plasmas **7**, 1845 (2000).
[20] T.-H. Watanabe and H. Sugama, Phys. Plasmas **9**, 3659 (2002).
[21] H. Hamada *et al.*, Fusion Eng. Des. **34−35**, 663 (1997).
[22] P. M. Schoch, K. A. Connor, D. R. Demers, and X. Zhang, Rev. Sci. Instrum. **74**, 1846 (2003).
[23] M. G. Shats and W. M. Solomon, Phys. Rev. Lett. **88**, 045001 (2002).
[24] G. S. Xu *et al.*, Phys. Rev. Lett. **91**, 125001 (2003).
[25] G. R. McKee *et al.*, Plasma Phys. Controlled Fusion **45**, A477 (2003).
[26] R. A. Moyer, G. R. Tynan, C. Holland, and M. J. Burin, Phys. Rev. Lett. **87**, 135001 (2001).
[27] P. H. Diamond *et al.*, Phys. Rev. Lett. **84**, 4842 (2000).
[28] A. Fujisawa *et al.*, Rev. Sci. Instrum. **67**, 3099 (1996).
[29] A. Fujisawa *et al.*, Phys. Rev. Lett. **82**, 2669 (1999).